



1 Article

2 **Cardiomyocyte apoptosis contributes to contractile dysfunction** 3 **in stem cell model of *MYH7* E848G hypertrophic cardi-** 4 **omyopathy**

5 **Alexander M. Loiben**^{1,2,3}, **Wei-Ming Chien**^{1,2,3,4}, **Clayton E. Friedman**^{1,2,3}, **Leslie S-L. Chao**^{1,2,3}, **Gerhard Weber**³,
6 **Alex Goldstein**^{1,2,3,5,7}, **Nathan Sniadecki**^{1,2,3,5,6,7}, **Charles E. Murry**^{1,2,3,6,7}, **Kai-Chun Yang**^{1,2,3,4*}

7 ¹ Institute for Stem Cell and Regenerative Medicine, University of Washington, School of Medicine, Seattle,
8 WA, USA

9 ² Center for Cardiovascular Biology, University of Washington, Seattle, WA, USA

10 ³ Department of Medicine/Cardiology, University of Washington, Seattle, WA, USA

11 ⁴ Cardiology/Hospital Specialty Medicine, VA Puget Sound HCS, Seattle, WA, USA

12 ⁵ Department of Mechanical Engineering, University of Washington, Seattle, WA, USA

13 ⁶ Department of Bioengineering, University of Washington, Seattle, WA, USA

14 ⁷ Department of Lab Medicine and Pathology, University of Washington, Seattle, WA, USA

15 * Correspondence: kcyang@uw.edu; Tel.: 1-206-221-5061

17 **Abstract:** Missense mutations in myosin heavy chain 7 (*MYH7*) are a common cause of hyper-
18 trophic cardiomyopathy (HCM), but the molecular mechanisms underlying *MYH7*-based HCM re-
19 main unclear. In this work, we generated cardiomyocytes derived from isogenic human induced
20 pluripotent stem cells to model the heterozygous pathogenic *MYH7* missense variant, E848G, which
21 is associated with left ventricular hypertrophy and adult-onset systolic dysfunction. *MYH7*^{E848G/+} in-
22 creased cardiomyocyte size and reduced the maximum twitch forces of engineered heart tissue,
23 consistent with the systolic dysfunction in *MYH7* E848G HCM patients. Interestingly, *MYH7*^{E848G/+}
24 cardiomyocytes more frequently underwent apoptosis that was associated with increased p53 ac-
25 tivity relative to controls. However, genetic ablation of *TP53* did not rescue cardiomyocyte survival or
26 restore engineered heart tissue twitch force, indicating *MYH7*^{E848G/+} cardiomyocyte apoptosis and
27 contractile dysfunction are p53-independent. Overall, our findings suggest that cardiomyocyte
28 apoptosis plays an important role in the *MYH7*^{E848G/+} HCM phenotype *in vitro* and that future efforts
29 to target p53-independent cell death pathways may be beneficial for the treatment of HCM patients
30 with systolic dysfunction.

31 **Keywords:** Hypertrophic cardiomyopathy, dilated cardiomyopathy, *MYH7*, p53, engineered heart
tissue, apoptosis, contractile dysfunction, induced pluripotent stem cells

Citation: To be added by editorial staff during production.

Academic Editor: Firstname
Lastname

Received: date

Revised: date

Accepted: date

Published: date



Copyright: © 2023 by the authors

Submitted for possible open access

publication under the terms and

conditions of the Creative Commons

Attribution (CC BY) license

(<https://creativecommons.org/licenses/by/4.0/>)

1. Introduction

Hypertrophic cardiomyopathy (HCM), characterized by unexplained left ventricular hypertrophy, affects 1 in 500 individuals in the general population [1,2]. While the left ventricular function is generally preserved to hyperdynamic, it is increasingly realized that the primary defect in some cases is impaired contractile function [1,2,3,4,5,6]. Mutations in myosin heavy chain 7 (*MYH7*), encoding a sarcomeric thick filament protein, are common genetic causes for HCM, accounting for 33% of cases [7,8]. Recently, mavacamten, a myosin inhibitor, was found to improve symptoms in HCM patients with preserved to hyperdynamic systolic function and left ventricular outflow tract obstruction by reducing contractility; however, mavacamten is contraindicated in patients with reduced ejection fraction as it can further worsen systolic function [9]. Because ~10% of HCM patients develop systolic dysfunction, this class of medication is not an option for them [9,10]. In order to develop novel therapies for patients with HCM and systolic dysfunction, a better understanding of the molecular mechanisms that govern this disease is needed.

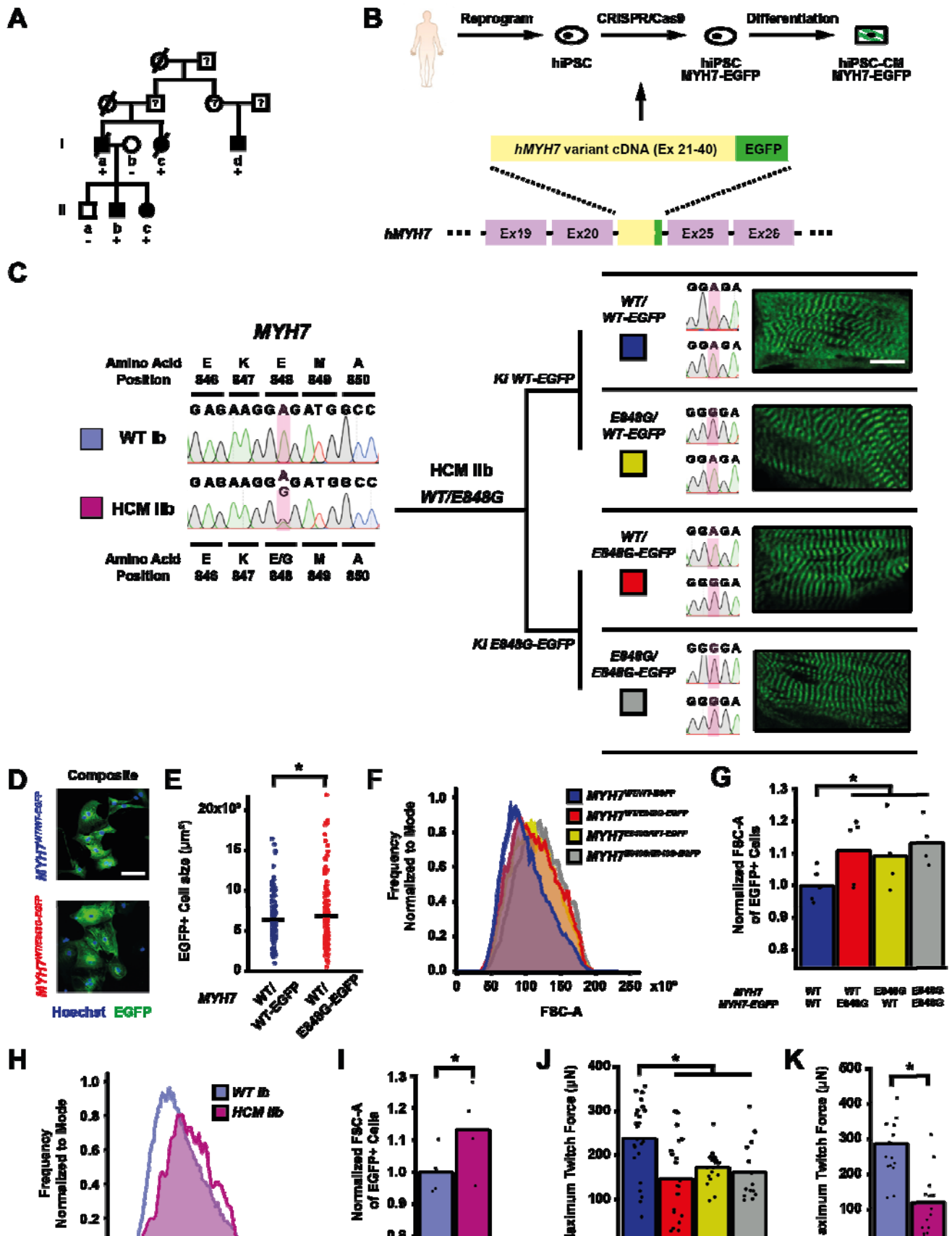
49 Cardiomyocyte apoptosis has been observed in various models of cardiac diseases
50 [11,12,13,14,15,16]. The activation of tumor suppressor p53, a major driver of intrinsic
51 apoptosis, has been implicated in the progression of cardiac hypertrophy at both the
52 cellular and tissue level [17,18,19,20,21,22,23,24]. In an hiPSC-CM model of the
53 MYH7^{R403Q/+} HCM associated with hypercontractile function, p53 inhibition partially res-
54 cued cardiomyocyte survival but did not normalize the hypercontractile function in cardiac
55 microtissues [17]. Given that the role of p53 in HCM associated with hypocontractile
56 function is unknown, we hypothesize that inhibition of p53 in this setting will improve
57 cardiomyocyte survival and overall contractile function.

58 In previous work, patients harboring the heterozygous MYH7E848G/+ variant pre-
59 sented with adult-onset familial systolic dysfunction and mild ventricular wall thickening
60 [6]. Since that publication, an additional family member presented with significant left
61 ventricular hypertrophy that met criteria for HCM, which diagnoses the rest of the
62 MYH7E848G/+ family members exhibiting at least 1.3 cm wall thickening with HCM as per
63 the 2020 American College of Cardiology and American Heart Association HCM Guide-
64 lines [25]. Thus, MYH7E848G/+ hiPSC-CM is an ideal model for testing the role of p53 in
65 HCM associated with hypocontractile function. Here, we improve upon the prior viral
66 transgenesis approach using CRISPR/Cas9 editing of patient-derived hiPSCs to generate
67 isogenic lines expressing MYH7-EGFP fusion proteins with the E848G variant to better
68 understand the pathophysiology of MYH7E848G/+ based HCM associated with
69 hypocontractile function. This model recapitulated the clinical phenotype as we observed
70 increased cardiomyocyte hypertrophy and decreased tissue contractility in both pa-
71 tient-derived and isogenic hiPSC-CMs expressing MYH7E848G/+. In cardiomyocytes
72 derived from the hiPSCs, we found that the MYH7 E848G allele increased cytotoxicity,
73 apoptosis markers, and p53 expression, but genetic ablation of TP53 did not restore
74 contractile function or cardiomyocyte survival. Overall, our findings suggest in HCM pa-
75 tients with systolic dysfunction, cardiomyocyte apoptosis contributes to impaired tissue
76 contractility with p53-independent cell death as a potential mechanism.

77 2. Results

78 2.1. Generation of isogenic β MHC-EGFP expressing hiPSC-CMs using CRISPR/Cas9 79 editing

80 Since the publication of our last study, another family member in the original study
81 presented (patient II d) with clear left ventricular septal wall thickening on echo (1.9 cm)
82 and severe LV systolic dysfunction (EF 39%) at age 57 [6] (Fig. 1a). Based on the diag-
83 nostic criteria for HCM as recommended, because one family member has clear HCM
84 phenotype, the rest of the MYH7 E848G family members with at least 1.3 cm wall thick-
85 ening would now meet diagnostic criteria for HCM (patient Ia) [25]. To study the effects of
86 MYH7^{E848G/+} variant in the context of isogenic gene-edited hiPSCs *in vitro*, we leveraged
87 previously generated human induced pluripotent stem cells (hiPSCs) derived from an
88 HCM patient (HCM II b) and a non-variant family member (WT Ib) (Fig. 1a). To generate
89 isogenic hiPSC lines with fluorescent tracking of β MHC, the protein encoded by MYH7, we
90 designed a gene editing strategy to create hiPSC lines expressing β MHC-EGFP fusion
91 proteins (Fig. 1b, Fig. S1a). Enrichment with the mPGK-puromycin cassette improved the
92 gene-editing efficiency such that ~10% of the colonies screened were correct (Fig. S1a).
93 By knocking MYH7 cDNA in-frame with the sequence of eGFP into the endogenous MYH7
94 locus of HCM II b MYH7^{E848G/+} hiPSCs, we enabled direct native control of the expression
95 and tracking of the β MHC -EGFP fusion protein (Fig. S1a). With this approach, we gen-
96 erated four isogenic β MHC -EGFP expressing hiPSC lines with all combinations of WT
97 and E848G homozygous and heterozygous alleles with one allele EGFP-tagged:



99
100
101
102
103
104
105
106
107
108
109
110
111
112
113
114
115
116
117
118
119

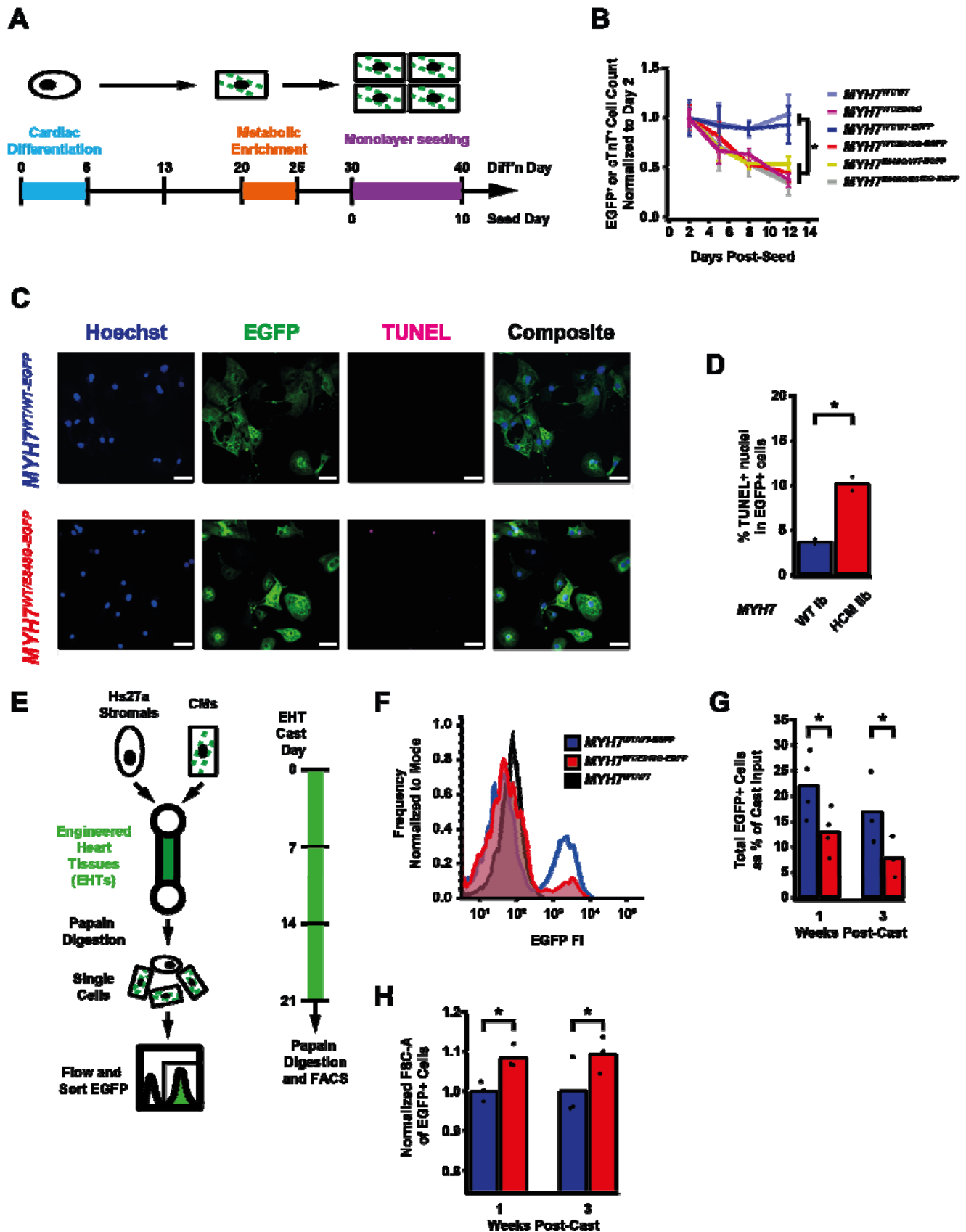
Figure 1. *MYH7* E848G increases cardiomyocyte size and reduces engineered heart tissue contractility in human stem cell model. **(a)** Family pedigree for *MYH7* E848G. (+), WT/E848G; (-), WT/WT; black, HCM; white, no HCM. **(b)** Schematic of CRISPR/Cas9 gene editing strategy to generate isogenic hiPSC-CMs expressing *MYH7-EGFP* fusion protein under control of endogenous *MYH7* locus. **(c)** (L) Sanger sequencing chromatograms of *MYH7* Exon 22 for patient-derived hiPSCs. (R) Schematic of relationship between isogenic hiPSC-CM lines, with Sanger sequencing chromatograms of *MYH7* Exon 22 and representative confocal microscopy images of sarcomeric striations at differentiation day 35. Scale bar 10 μm . **(d)** Representative confocal microscopy images for Hoechst-stained *MYH7*^{WT/WT-EGFP} and *MYH7*^{WT/E848G-EGFP} hiPSC-CMs, differentiation day 33. Scale bar 100 μm . **(e)** 2D area of EGFP⁺ *MYH7*^{WT/WT-EGFP} and *MYH7*^{WT/E848G-EGFP} hiPSC-CMs, differentiation day 33, from confocal images. Mean and cell replicates shown, n = 150 cells. **(f)** Representative histogram of forward scatter area (FSC-A) as measured by flow cytometry of isogenic hiPSC-CMs, differentiation day 40. n = 10,000 cells. **(g)** Normalized FSC-A as measured by flow cytometry of EGFP⁺ isogenic hiPSC-CMs, differentiation day 42. Mean and biological replicates shown. **(h)** Representative histogram of forward scatter area (FSC-A) as measured by flow cytometry of patient-derived hiPSC-CMs, differentiation day 40. n = 10,000 cells **(i)** Normalized FSC-A as measured by flow cytometry of cTnT⁺ patient-derived hiPSC-CMs, differentiation day 42. Mean and biological replicates shown. **(j)** Maximum twitch force of EHTs at cast week 3 for isogenic hiPSC-CMs. Mean and tissue replicates shown. **(k)** Maximum twitch force of EHTs at cast week 3 for patient-derived hiPSC-CMs. Mean and tissue replicates shown. * in (e,g,i-k) indicates p < 0.05 significance calculated by Student's t-test.

120
121
122
123
124
125
126
127
128
129
130
131
132
133
134
135
136
137
138
139
140
141
142
143
144
145
146
147
148
149
150
151
152
153
154

MYH7^{WT/WT-EGFP}, *MYH7*^{WT/E848G-EGFP}, *MYH7*^{E848G/WT-EGFP}, and *MYH7*^{E848G/E848G-EGFP} (Fig. 1c). Notably, our editing approach yielded successfully edited clones as verified by Sanger sequencing with high efficiency, with cumulatively 10 of 76 picked clones (13.2%) across the four lines (Fig. S1b) correctly gene-edited. Green striated sarcomeres were visible in confocal microscopy in each line upon successful differentiation into hiPSC-CMs (Fig. 1c). Western blot confirmed the presence of two β MHC protein bands of roughly equal intensity, corresponding with untagged and EGFP-tagged β MHC (Fig. S1c), suggesting no preferential expression of one allele over the other. The establishment of these hiPSC-CM lines enabled various lines of inquiry related to the effects of *MYH7*^{E848G/+} on cardiomyocyte behavior *in vitro*, while also providing evidence of the utility of our approach for creating multiple edits to study a *MYH7* variant.

2.2. *MYH7*^{E848G/+} variant increases cell size and reduces tissue contractility in hiPSC-CMs

First, we sought to address whether our *MYH7-EGFP* lines recapitulated *in vitro* the key measures of hypertrophy and hypocontractility present *in vivo*. *MYH7*^{WT/WT-EGFP} and *MYH7*^{WT/E848G-EGFP} hiPSC-CMs were seeded for 7 days in monolayer on Matrigel. Immunocytochemistry revealed significantly increased *MYH7*^{WT/E848G-EGFP} two-dimensional projected area (3100 \pm 170 μm^2) relative to *MYH7*^{WT/WT-EGFP} projected area (2870 \pm 110 μm^2), an 8.0% increase (Fig. 1D-E). This finding is consistent with a previously reported increase of 10% in cell size in *MYH7*^{R403Q/+} hiPSC-CMs [17]. All three isogenic E848G-expressing lines exhibited increased forward scatter area (11.1 \pm 4.6%, 9.4 \pm 5.8 %, 13.4 \pm 3.7 % increase) relative to *MYH7*^{WT/WT-EGFP} as measured by flow cytometry (Fig. 1f-g), confirming the immunocytochemistry findings. This matches the cellular hypertrophy observed in patient-derived hiPSC-CMs, as HCM IIb cardiomyocytes also had increased forward scatter area (13.2 \pm 6.9% increase) relative to WT Ib cardiomyocytes (Fig. 1h-i). To assess tissue contractility, we used the K3 configuration of three-dimensional engineered heart tissues (EHTs) on flexible PDMS microposts (Fig. S1d), which approximates moderate afterload as previously described [26]. The maximum twitch force at week 3 of EHT casting was significantly weaker in all three isogenic E848G-expressing lines (147.0 \pm 19.5 μN , 173.0 \pm 8.4 μN , 161.7 \pm 18.0 μN) relative to *MYH7*^{WT/WT-EGFP} (238.2 \pm 17.4 μN) (Fig. 1j). With patient-derived hiPSC-CMs, the maximum twitch force at week 3 of EHT casting was also significantly weaker in HCM IIb EHTs (118.9 \pm 23.7 μN) relative to WT Ib EHTs (287.4 \pm 27.7 μN), mirroring the findings in EHTs with the isogenic lines (Fig. 1k). In sum, our isogenic and patient-derived *MYH7* E848G lines demonstrated both cardiomyocyte hypertrophy and tissue hypocontractility, thus serving as a useful *in vitro* model of *MYH7*^{E848G/+} HCM.



156 **Figure 2.** *MYH7*^{E848G} reduces hiPSC-CM survival in monolayer and EHT culture. (a) Schematic
157 of iPSC-CM differentiation and seeding protocol for monolayer culture. (b) Total EGFP⁺ cell count
158 for isogenic hiPSC-CMs and cTnT⁺ cell count for patient-derived hiPSC-CMs in DMEM-based
159 monolayer culture, normalized to day 2 post-seed. Mean ± SEM, n = 4-6 biological replicates. (c)
160 Representative confocal microscopy images for Hoechst- and TUNEL-stained *MYH7*^{WT/WT-EGFP} and
161 *MYH7*^{WT/E848G-EGFP} hiPSC-CMs, differentiation day 33. Scale bar 50 μm. (d) Quantification of per-
162 centage of TUNEL⁺ nuclei in EGFP⁺ hiPSC-CMs from (l), n = 2 biological replicates shown, n = 150
163 cells per replicate. * indicates p < 0.05 significance calculated by Student's t-test. (e) Schematic for
164 casting protocol for engineered heart tissues (EHTs) and papain-based digestion for FACS-based
165 analysis. (f) Representative histogram of EGFP intensity as measured by flow cytometry in
166 *MYH7*^{WT/WT}, *MYH7*^{WT/WT-EGFP}, *MYH7*^{WT/E848G-EGFP} EHTs, cast week 1, n = 10,000 cells. (g) Total
167 EGFP⁺ cells as percentage of initial EHT cast input for *MYH7*^{WT/WT-EGFP} and *MYH7*^{WT/E848G-EGFP}
168 EHTs, cast week 1 and 3, as measured by FACS. Mean and cast replicates shown, 3-6 tissues per
169 cast. (h) Normalized FSC-A of EGFP⁺ cells in *MYH7*^{WT/WT-EGFP} and *MYH7*^{WT/E848G-EGFP} EHTs, cast
170 week 1 and 3, as measured by FACS. Mean and cast replicates shown, 3-6 tissues per cast. * in (b,
171 d, g-h) indicates p < 0.05 significance calculated by Student's t-test.

172 2.3. *MYH7*^{E848G/+} reduces hiPSC-CM survival in monolayer culture

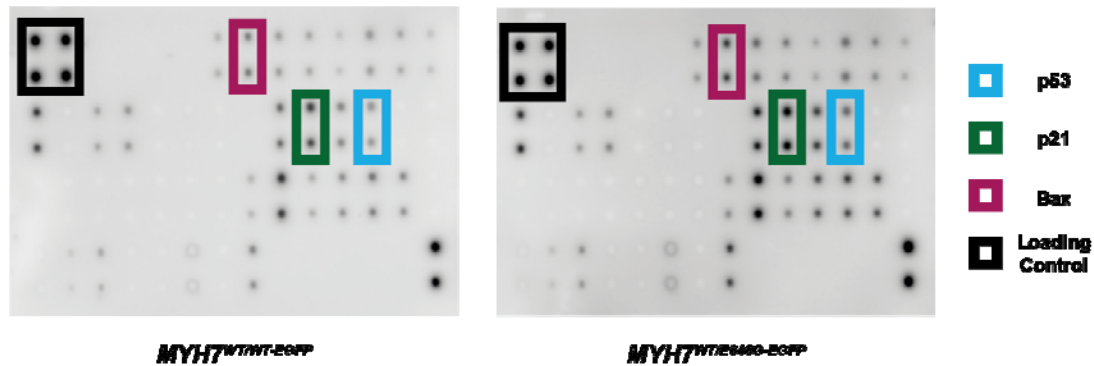
173 To expedite the maturation process and thus the expression and effects of
174 *MYH7*^{E848G/+} variant, we tested two different cardiomyocyte culture media: one with an
175 RPMI base and low calcium concentration (0.4 mM Ca²⁺), and one with a DMEM base and
176 more approximately physiological calcium concentration (1.8 mM Ca²⁺). After 10 days of
177 treatment, EGFP intensity as measured by flow cytometry was significantly increased for
178 *MYH7*^{WT/WT-EGFP} iPSC-CMs cultured in DMEM-based media (93.6 ± 3.2% increase) rela-
179 tive to those in RPMI-based media (Fig. S2a-b); FSC area also increased with
180 DMEM-based media (13.9 ± 8.0% increase) relative to RPMI-based media (Fig. S2c),
181 suggesting increased maturation with the DMEM-based high calcium media. Moving
182 forward, we used this DMEM-based media for all monolayer experiments.

183 While culturing the *MYH7*^{E848G/+} cardiomyocytes, we noted a significant loss of the
184 mutant cardiomyocytes during prolonged culture (Fig. 2a). WT Ib and HCM Ib patient
185 lines and *MYH7-EGFP* isogenic lines were monolayer cultured for two weeks in
186 DMEM-based media. Intriguingly, lines without *MYH7* E848G had negligible difference in
187 cTnT⁺ or EGFP⁺ total cell count over time, but those with *MYH7* E848G had significant
188 reduction in cTnT⁺ or EGFP⁺ total cell count (Fig. 2b). To further explore the manner of cell
189 death, *MYH7*^{WT/WT-EGFP} and *MYH7*^{WT/E848G-EGFP} hiPSC-CMs were stained with terminal
190 deoxynucleotidyl transferase dUTP nick end labeling (TUNEL). The fraction of TUNEL⁺
191 nuclei in EGFP⁺ cells after 3 days DMEM-based media treatment was significantly higher
192 in *MYH7*^{WT/E848G-EGFP} (10.2 ± 0.8%) relative to *MYH7*^{WT/WT-EGFP} hiPSC-CMs (3.7 ± 0.3%),
193 suggesting apoptosis was the cause of cell death (Fig. 2c-d). Combined, these data indi-
194 cate *MYH7*^{E848G/+} reduces hiPSC-CM viability when cultured on a stiff tissue culture
195 surface, suggesting that the *MYH7*^{E848G/+} cardiomyocytes may be susceptible to increased
196 afterload.

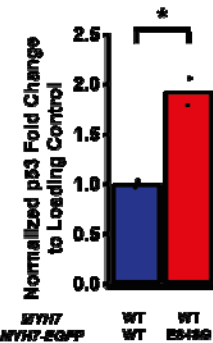
197 2.4. *MYH7*^{E848G/+} reduces hiPSC-CM survival and increases cardiomyocyte size in EHTs

198 We posited the reduced monolayer viability of *MYH7*^{E848G/+} may translate to the EHT
199 environment and help explain the impaired hypocontractility phenotype. Thus, we utilized
200 a previously described method for papain-based digestion of EHTs into single cells for
201 analysis with flow assisted cell sorting (FACS) (Fig. 2e) [27]. There was a significant de-
202 crease in the EGFP⁺ fraction of the sorted EHT population in *MYH7*^{WT/E848G-EGFP} tissues at
203 both 1 week (13.2 ± 6.0%) and 3 weeks (7.6 ± 0.7%) post-cast, relative to the EGFP⁺
204 fraction in *MYH7*^{WT/WT-EGFP} tissues (27.4 ± 0.9%, 20.9 ± 1.6%) as detected by flow
205 cytometry (Fig. f-g). Although cardiomyocyte loss was persistent over time in the EHTs,
206 there was differential survival in the 1st week of culture that was not seen between 1 and 3
207 weeks of culture in EHTs, indicating that once the EHTs had compacted to steady state,
208 the *MYH7*^{E848G/+} cardiomyocytes no longer exhibit increased cytotoxicity compared to the
209 control line. This is in contrast to when the cardiomyocytes were plated on stiff tissue
210 culture plastic where we found persistent genotype-dependent decrease in survival over
211 time (Figure 2b), further suggesting that the genotype-dependent cardiomyocyte apopto-
212 sis is in part due to afterload. We next examined if the cardiomyocytes exhibited a hy-
213 pertrophic response in the 3D environment. *MYH7*^{WT/E848G-EGFP} EHTs yielded EGFP⁺
214 cardiomyocytes with increased forward scatter area (8.4 ± 1.7% increase) relative to those
215 sorted from *MYH7*^{WT/WT-EGFP} EHTs (Fig. 2h), indicating an E848G-induced hypertrophic
216 response was also present in the 3D environment.

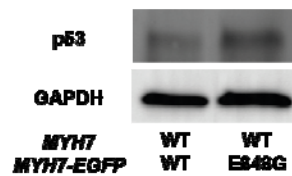
A



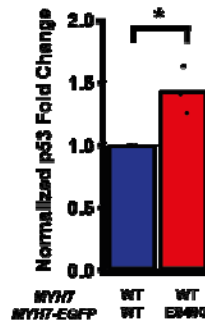
B



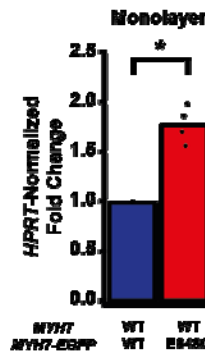
C



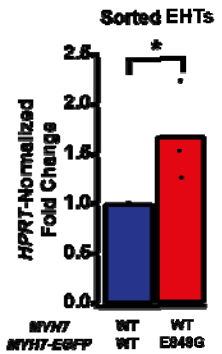
D



E



F



217

218

219

220

221

222

223

224

225

226

227

228

229

230

Figure 3. *MYH7* E848G induces p53-associated intrinsic apoptosis in monolayer and EHT culture. (a) Human apoptosis antibody array for *MYH7*^{WT/WT-EGFP} and *MYH7*^{WT/E848G-EGFP} hiPSC-CMs, differentiation day 35, with select targets highlighted. (b) Quantification of protein expression from (A) normalized to loading control and *MYH7*^{WT/WT-EGFP}. Mean and biological replicates shown, n = 2 technical replicates. (c) Representative western blot for p53 and α -sarcomeric actinin protein expression in *MYH7*^{WT/WT-EGFP} and *MYH7*^{WT/E848G-EGFP} hiPSC-CMs, differentiation day 40. (d) Quantification of p53 protein expression from (c) normalized to α -sarcomeric actinin and *MYH7*^{WT/WT-EGFP}. Mean and biological replicates shown. (e) *TP53* mRNA expression for *MYH7*^{WT/WT-EGFP} and *MYH7*^{WT/E848G-EGFP} hiPSC-CMs normalized to *HPRT* and *MYH7*^{WT/WT-EGFP}, differentiation day 40, as measured by RT-qPCR. Mean and biological replicates shown. (f) *TP53* mRNA expression for *MYH7*^{WT/WT-EGFP} and *MYH7*^{WT/E848G-EGFP} EGFP⁺ hiPSC-CMs sorted from cast week 1 EHTs, normalized to *HPRT* and *MYH7*^{WT/WT-EGFP}, as measured by RT-qPCR. Mean and biological replicates shown. * in (b, d-f) indicates p < 0.05 significance calculated by Student's t-test.

231

232

2.5. p53 and associated markers of intrinsic apoptosis are elevated in *MYH7*^{WT/E848G-EGFP} hiPSC-CMs

233

234

235

236

237

238

239

240

241

242

243

244

245

Given the TUNEL results and the reduced survival of *MYH7*^{WT/E848G-EGFP} hiPSC-CMs in both monolayer and EHT environments, we decided to further explore apoptotic signaling. As such, we tested *MYH7*^{WT/WT-EGFP} and *MYH7*^{WT/E848G-EGFP} hiPSC-CMs with 5 days of DMEM-based media treatment on a human apoptosis antibody array for 43 protein targets (Fig. 3A). We saw significant upregulation of p53 (92.8 \pm 2.8% increase) and associated downstream signaling elements p21 (66.3 \pm 9.9% increase) and Bax (55.8 \pm 10.9% increase) in *MYH7*^{WT/E848G-EGFP} relative to *MYH7*^{WT/WT-EGFP}, suggesting p53 pathway activity is elevated in hiPSC-CMs by the *MYH7* E848G variant (Fig. 3b, S3a-b, Table 1), p53 protein expression remained elevated (43.2 \pm 11.0% increase) in *MYH7*^{WT/E848G-EGFP} hiPSC-CMs after 10 days of DMEM-based media treatment, corroborating the results of the apoptosis antibody array (Fig. 3c-d). Notably, we did not see significant differences in TNF α , TNF β , or FasL, ruling out extrinsic apoptosis as a mechanism for reduced viability (Table 1). At the transcriptional level, *TP53* expression was elevated after 10 days of

246 DMEM-based media treatment in $MYH7^{WT/E848G-EGFP}$ hiPSC-CMs ($78.1 \pm 9.3\%$ increase)
 247 relative to $MYH7^{WT/WT-EGFP}$, suggesting p53 upregulation is due to increased transcrip-
 248 tional activity (Fig. 3e). In EHTs, FACS-sorted EGFP⁺ cells from $MYH7^{WT/E848G-EGFP}$ tissues
 249 had higher TP53 expression ($67.0 \pm 29.0\%$ increase) relative to those from
 250 $MYH7^{WT/WT-EGFP}$ tissues (Fig. 3f). In sum, $MYH7^{E848G/+}$ hiPSC-CMs in both 2D and 3D
 251 contexts have elevated p53 signaling activity that is associated with increased
 252 cardiomyocyte apoptosis.

253 **Table 1.** Apoptosis antibody array results. Mean fold change of $MYH7^{WT/E848G-EGFP}$ relative to
 254 $MYH7^{WT/WT-EGFP}$, n = 2 biological and n = 2 technical replicates per target.

Target	Mean	SEM
Bad	1.5352	0.1057
Bax	1.5582	0.1091
Bcl-2	1.6521	0.1741
Bcl-w	1.5401	0.1135
BID	1.5019	0.2071
BIM	1.4059	0.0426
Caspase 3	1.5923	0.0832
Caspase 8	1.4939	0.0764
CD40	1.0415	0.0849
CD40L	Undetected	Undetected
clAP-2	1.1889	0.0648
cytoC	1.2351	0.1035
DR6	Undetected	Undetected
Fas	Undetected	Undetected
FasL	Undetected	Undetected
HSP27	1.7363	0.0837
HSP60	1.5025	0.0892
HSP70	1.8451	0.1159
HTRA	1.5470	0.0832
IGF-1sR	Undetected	Undetected
IGFBP-1	Undetected	Undetected
IGFBP-2	Undetected	Undetected
IGFBP-3	Undetected	Undetected
IGFBP-4	Undetected	Undetected
IGFBP-5	Undetected	Undetected
IGFBP-6	Undetected	Undetected
IGF-I	Undetected	Undetected
IGF-II	Undetected	Undetected
Livin	1.7624	0.0648
p21	1.6627	0.0993
p27	1.7597	0.0796
p53	1.9283	0.0279
SMAC	1.6109	0.0511
sTNF-R1	Undetected	Undetected
sTNF-R2	Undetected	Undetected
Survivin	1.9151	0.0921

TNF α	1.0003	0.0383
TNF β	1.3673	0.0586
TRAILR-1	Undetected	Undetected
TRAILR-2	Undetected	Undetected
TRAILR-3	1.7914	0.1804
TRAILR-4	Undetected	Undetected
XIAP	1.8136	0.0887

255

256

257

2.6. *TP53* ablation does not rescue contractile function, cardiomyocyte survival, or cellular hypertrophy in EHTs with *MYH7*^{E848G/+} hiPSC-CMs

258

259

260

261

262

263

264

265

266

267

268

269

270

271

272

273

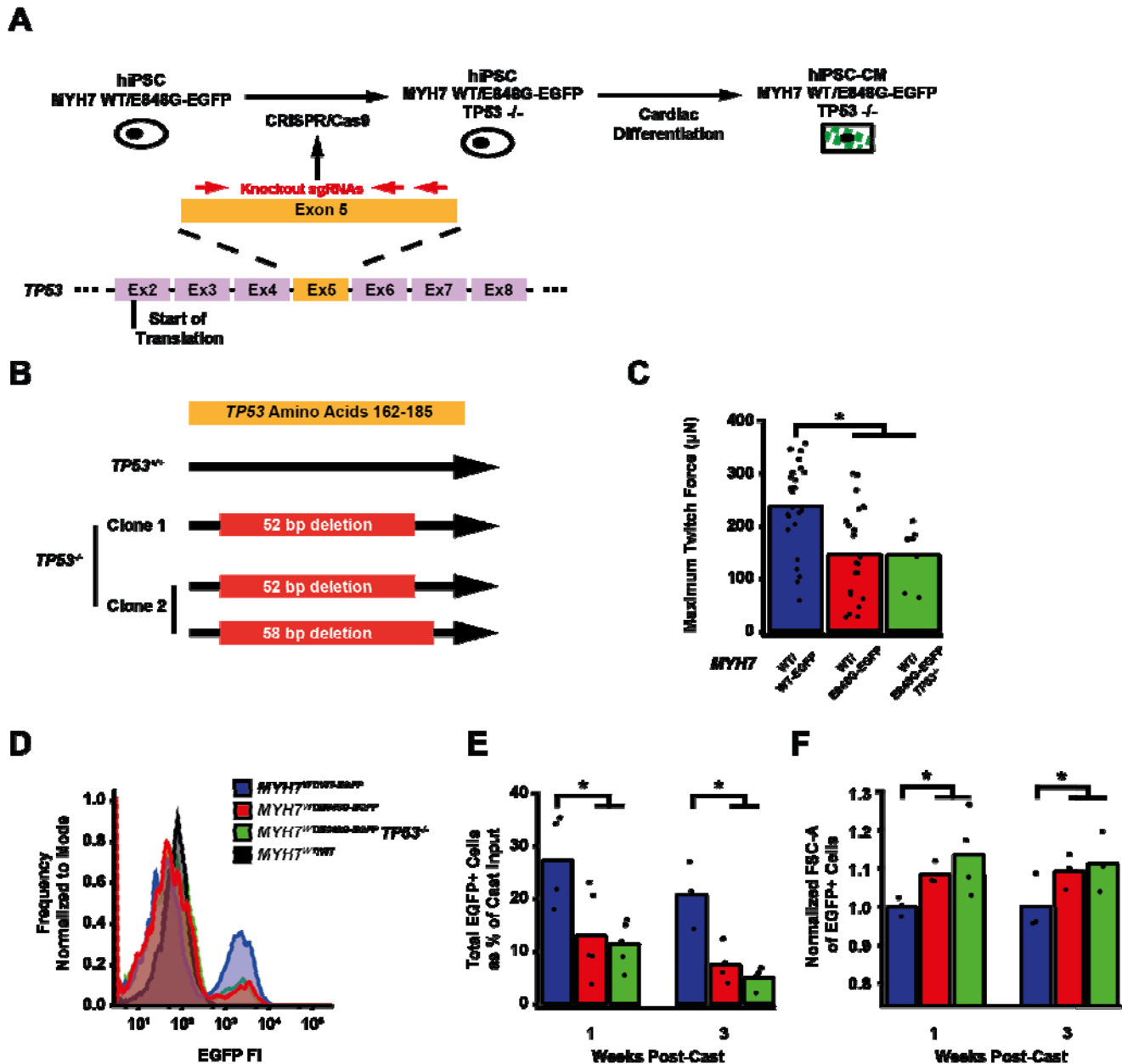
274

275

276

277

We sought to determine whether p53 activity was necessary for the observed effects of *MYH7*^{E848G/+} on contractility and cardiomyocyte survival in our *MYH7-EGFP* hiPSC-CM EHT model. Thus, we used CRISPR/Cas9 gene editing to knock out *TP53* in *MYH7*^{WT/E848G-EGFP} hiPSCs, generating a new *MYH7*^{WT/E848G-EGFP} *TP53*^{-/-} hiPSC line (Fig. 4a). Three sgRNAs targeting Exon 5 of *TP53* were used to ablate both *TP53* alleles as evidenced by Sanger sequencing (Fig. 4b, S4a). Notably, *MYH7*^{WT/E848G-EGFP} *TP53*^{-/-} EHTs (146.4 \pm 21.6 μ N) had no significant difference in maximum contractile force relative to *TP53*^{+/+} EHTs at cast week 3 (147.0 \pm 19.5 μ N), indicating p53 activity is not driving impaired contractility in our model (Fig. 4c). When these EHTs were sorted by FACS, EGFP⁺ percentage at cast week 1 (11.5 \pm 4.5%, n = 4 casts) and total EGFP⁺ counts (47,100 \pm 8300 EGFP⁺ cells) in *TP53*^{-/-} EHTs were similar to those in *TP53*^{+/+} EHTs (13.2 \pm 6.0%, 49,700 \pm 14,600 EGFP⁺ cells), indicating cardiomyocyte survival was unaffected by ablating p53 activity (Fig. 4d-e). Cast week 3 *TP53*^{-/-} EHTs (5.1 \pm 1.9%, 22,800 \pm 4600 EGFP⁺ cells) remained indistinguishable from corresponding *TP53*^{+/+} EHTs (7.6 \pm 0.7%, 26,000 \pm 6100 EGFP⁺ cells). Increased forward scatter area of EGFP⁺ cardiomyocytes in *TP53*^{+/+} EHTs (8.4 \pm 1.8% increase) persisted in *TP53*^{-/-} EHTs (13.6 \pm 5.3% increase), indicating *TP53* ablation does not rescue cellular hypertrophy (Fig. 4f). Thus, p53 activity does not appear to be necessary for reduced contractility, cardiomyocyte cytotoxicity, or cellular hypertrophy in our *MYH7-EGFP* hiPSC-CM EHT model, and specific targeting of p53 does not restore healthy phenotype.



278

279

280

281

282

283

284

285

286

287

288

289

290

Figure 4. TP53 ablation does not rescue contractile function, hypertrophy, or cardiomyocyte survival in MYH7 E848G expressing hiPSC-CMs. (a) Schematic of CRISPR/Cas9 gene editing strategy to generate MYH7^{WT/E848G-EGFP} TP53^{-/-} hiPSC-CMs. (b) Schematic of deletions in MYH7^{WT/E848G-EGFP} TP53^{-/-} clones. (c) Maximum twitch force of EHTs at cast week 3 for isogenic hiPSC-CMs. Mean and tissue replicates shown. (d) Representative histogram of EGFP intensity as measured by flow cytometry in MYH7^{WT/WT}, MYH7^{WT/WT-EGFP}, MYH7^{WT/E848G-EGFP}, and MYH7^{WT/E848G-EGFP} TP53^{-/-} EHTs, cast week 1. n = 10,000 cells. (e) Total EGFP⁺ cells as percentage of initial EHT cast input for MYH7^{WT/WT-EGFP}, MYH7^{WT/E848G-EGFP}, and MYH7^{WT/E848G-EGFP} TP53^{-/-} EHTs, cast week 1 and 3, as measured by FACS. Mean and cast replicates shown, 3-6 tissues per cast. (f) Normalized FSC-A of EGFP⁺ cells in MYH7^{WT/WT-EGFP}, MYH7^{WT/E848G-EGFP}, and MYH7^{WT/E848G-EGFP} TP53^{-/-} EHTs, cast week 1 and 3, as measured by FACS. Mean and cast replicates shown, 3-6 tissues per cast. * in (c, e-f) indicates p < 0.05 significance calculated by Student's t-test.

291

292

3. Discussion

293 In this work, we generated isogenic hiPSCs with MYH7-EGFP fusion expression in
294 the endogenous *MYH7* locus, with or without the *MYH7*^{E848G/+} variant. Our editing ap-
295 proach provides a couple advantages. First, the use of patient-derived hiPSCs with het-
296 erozygous *MYH7*^{E848G/+} as the parental cell line ensured the corrected and variant isogenic
297 lines have the same patient-derived genetic background. Approaches which use previ-
298 ously established wild-type lines as the base cell line do not capture the same genetic
299 background as a patient-derived model. Second, this gene-editing strategy leverages an
300 antibiotic enrichment cassette that significantly reduces the number of colonies needed to
301 be screened, thereby permitting the generation of multiple isogenic hiPSC lines with
302 *MYH7* variants.

303 In our isogenic hiPSC-CM model, *MYH7*^{E848G/+} increased cell size, reduced
304 cardiomyocyte survival, and reduced tissue contractility in three-dimensional culture.
305 These findings correlated with reduced survival, cellular hypertrophy, and impaired tissue
306 contractility in our patient-derived non-fluorescent hiPSC-CM lines. The cellular hyper-
307 trophy and decrease in cardiomyocyte survival has been reported in an hiPSC-CM model
308 of the *MYH7*^{R403Q/+} HCM associated with hypercontractile function [17]. In that study, p53
309 activity was elevated and inhibition with the small molecule pifithrin partially rescued
310 cardiomyocyte survival, but it did not normalize contractile function. We also observed
311 increased p53 activity in our hypocontractile HCM model, and we genetically ablated *TP53*
312 to interrogate the role of p53. To our knowledge, this is the first study to fully ablate *TP53*
313 expression in the context of HCM-associated cytotoxicity and impaired tissue contractility.
314 We believe genetic ablation provides a definitive answer on the role of p53 in *MYH7*^{E848G/+}
315 HCM associated with systolic dysfunction compared to alternative methods that utilize
316 small molecules or viral transgenesis [17,21]. We have demonstrated reduced
317 cardiomyocyte survival and tissue hypocontractility are independent of p53 activity in our
318 model of HCM with hypocontractile function. This does not rule out p53's role in other
319 HCM-causative *MYH7* variants or other sarcomeric variants.

320 This work represents the first attempt to leverage EHT dissociation [27] to interrogate
321 hiPSC-CM survival, hypertrophy, and expression at a cellular level in the context of an
322 HCM-causative variant with hypocontractile function cultured in a 3D cardiac organoid.
323 Notably, *MYH7*^{E848G/+} increased cytotoxicity and cell size in the three-dimensional context,
324 demonstrating the variant effects in two-dimensional culture is also present in a more
325 relevant, 3D environment.

326 In sum, we have shown the *MYH7*^{E848G/+} HCM-causative variant associated with
327 hypocontractile function yields cardiomyocyte hypertrophy with reduced survival and tis-
328 sue contractility in a p53-independent manner, suggesting that future efforts to target
329 p53-independent apoptotic mechanisms may be beneficial for the treatment of HCM as-
330 sociated with hypocontractile function.

331 4. Materials and Methods

332 4.1. Monolayer culture of hiPSCs

333 hiPSCs were cultured in mTeSR+ (STEMCELL Technologies, 100-0276) supple-
334 mented with 50 U/mL penicillin/streptomycin (Invitrogen, 15140122) on plates coated with
335 80 µg/mL Matrigel (Corning, 356231, Lot 1242001) at 5% CO₂ and 37C. Cells were fed
336 every other day and passaged with 500 µM EDTA (Invitrogen, 15575-038) before differ-
337 entiation was morphologically evident. Media was supplemented with 10 µM ROCK in-
338 hibitor (SelleckChem, Y27632) for first 24 hours post-passage.

339 4.2. CRISPR/Cas9 editing of patient-derived hiPSCs

340 Patient-derived hiPSCs corresponding with non-variant *MYH7* (WT lb) and hetero-
341 zygous *MYH7*^{E848G/+} variant were previously generated [6]. 1000k pelleted hiPSCs were
342 mixed with 1 µL 10 µM SP-dCas9-VPR (Addgene, 63798), 9 µL Buffer R2 (STEMCELL
343 Technologies, 100-0691), 1 µL 30 µM of gRNA (Table 2), and 1.5 µg of
344 pJet-MYH7-EGFP-PGK-PuroR plasmid (Supp. File 1). For *TP53* ablation, pJet plasmid
345 was omitted. Cells were electroporated at 1400 V for 20 ms with a 10 µL tip using the Neon
346 Transfection System (Thermo Fisher, MPK5000). Transfected cells were plated in
347 mTeSR+ without penicillin/streptomycin supplemented with CloneR2 (STEMCELL
348 Technologies, 100-0691) and 10 µM ROCK inhibitor on plates coated with 80 µg/mL
349 Matrigel. Cells were fed every other day with mTeSR+ with 0.175 µg/mL puromycin
350 dihydrochloride (Thermo Fisher, A1113803) and replated at 88 cells/cm² in a 10 cm plate
351 coated with 80 µg/mL Matrigel for colony picking. Clones were replated in 96 well plates
352 for expansion and genomic DNA harvesting.

353

Table 2. sgRNA sequences for CRISPR/Cas9 editing.

Guide Target	Sequence
<i>MYH7</i>	UUCAUAUGAGCCCCUCCUGC
<i>MYH7</i>	GCCUUUGACACAAGAUUUUAG
<i>TP53</i>	CGCUAUCUGAGCAGCGCUCA
<i>TP53</i>	GUGCUGUGACUGCUUGUAGA
<i>TP53</i>	CAACAAGAUGUUUUGCCAAC

354

355

4.3. Generation of hiPSC-CMs

356

357

358

359

360

361

362

363

364

365

366

367

368

369

370

371

hiPSCs were seeded at 65k/cm² in mTeSR+ with 10 μM ROCK inhibitor on plates coated with 80 μg/mL Matrigel (Day -2). After 48 h (Day 0), media was replaced with RBA media [RPMI with L-glutamine (Invitrogen, 11875-119), 500 μg/mL bovine serum albumin (BSA; Sigma, A9418-50G), 213 μg/mL ascorbic acid (Sigma, A8960-5G)] supplemented with 5 μM Chiron 99021 (Cayman Chemical, 13122). After 48 h (Day 2), media was replaced with RBA media supplemented with 2 μM Wnt C59 (SelleckChem, S7037). After 48 h (Day 4), media was replaced with unsupplemented RBA media. After 48 h (Day 6), media was replaced with RPMI-based cardiomyocyte media [RPMI with L-glutamine, B27 supplement with insulin (Invitrogen, 175044, Lot 2181371), 50 U/mL penicillin/streptomycin] and replaced every other day until Day 20. hiPSC-CMs were dissociated with 0.5% trypsin (Invitrogen, 15090046) in 500 μM EDTA with 25 μU DNase I (Sigma, 260913-25MU) and replated at 65k/cm² in RPMI-based cardiomyocyte media with 5% FBS on 20 μg/mL Matrigel-coated plates. hiPSC-CMs were metabolically enriched for 5 d with daily feeding with DMEM without glucose or L-glutamine (Invitrogen, F530S) supplemented with 4 mM Sodium L-lactate (Sigma, 71718-10G). hiPSC-CMs were frozen at Day 25 in Cryostor at -80C or immediately used for EHTs.

372

4.4. Monolayer culture of hiPSC-CMs

373

374

375

376

377

378

379

380

Day 25 hiPSC-CMs were thawed at 500k/cm² in RPMI-based cardiomyocyte media with 5% FBS on 10 μg/mL Matrigel-coated plates. Cells were fed with RPMI-based cardiomyocyte media on Day 26 and 28. On Day 30, hiPSC-CMs were dissociated with 0.5% trypsin in 500 μM EDTA with 25 μU DNase I and replated at 250k/cm² in RPMI-based cardiomyocyte media with 5% FBS on 10 μg/mL Matrigel-coated plates. After 24 h (Day 31) and every ensuing 48 h, cells were fed with DMEM-based cardiomyocyte media [DMEM with high glucose (Invitrogen, 10313021), B27 supplement with insulin, 50 U/mL penicillin/streptomycin].

381

4.5. Casting of engineered heart tissues (EHTs)

382

383

384

385

386

387

388

389

390

391

392

393

394

EHTs were cast on polydimethylsiloxane (PDMS) microposts as previously described (26,27). Briefly, Sylgard 184 Elastomer Base and Curing Agent (Dow, 1317318) were mixed at 10:1 ratio and cured in a custom 3D printed mold for 18 h at 65C, with one flexible post and one glass rod filled stiff post per set of posts, 6 posts per array. Cured post arrays were removed from the mold and trimmed of excess PDMS. 500k Day 25 hiPSC-CMs and 100k human Hs27a stromal cells were mixed with 3 U/mL thrombin from bovine plasma (Sigma, T4648) and 5 mg/mL bovine fibrinogen (Sigma, E8630) in 100 μL EHT media [sterile filtered RPMI, B27 supplement, 5 g/L aminocaproic acid (Sigma, A2 504-256-100G), penicillin/streptomycin]. The cell slurry was added into 2% agarose wells between posts in a 24 well plate and incubated for 80 min at 37C, 5% CO₂. 350 μL EHT media was added to the wells and tissues were incubated for 10 min at 37C, 5% CO₂. Posts were carefully moved to a fresh 24 well plate in 2 mL EHT media, and tissues were cultured on posts for 3 weeks with media change every other day.

395

4.6. Analysis of EHT contractile force

396

397

398

399

400

401

402

403

5 s videos of paced EHTs were analyzed as previously described (26,27). 24-well metal electrode trays with 2 mL Tyrode solution [1.8 mM calcium chloride (Sigma, C4901), 1.0 mM magnesium chloride (Sigma, 1374248), 5.4 mM potassium chloride (Fisher, P330-500), 140 mM sodium chloride (Sigma, S5886-1KG), 0.33 mM monobasic sodium phosphate (Fisher, P284-500), 10 mM HEPES (Invitrogen, 15630-080), 5 mM dextrose (Sigma, D9434) in H₂O] per well were incubated for 30 min at 37C, 5% CO₂. EHT post arrays were transferred to the electrodes and paced for 5 s with 1.5 Hz, 10 V, 20 ms pulses with 45 fps videos captured using live brightfield microscopy. Maximal twitch force was

404 calculated based on peak length displacement of tissues using previously published
405 MATLAB code.

406 **4.7. PCR amplification and sequencing**

407 Genomic DNA was isolated from hiPSC subclones using DNeasy Blood and Tissue
408 Kit (Qiagen, 69506). MYH7 fragment containing mutation was amplified by PCR using Q5
409 High-Fidelity DNA Polymerase (New England Biolabs, M0491L) and 500 nM forward and
410 reverse primers (Table 3). PCR products were run on 1% agarose gels and extracted
411 using Fermentas Gel Extraction Kit (Invitrogen, K0692). Sanger sequencing was per-
412 formed by Eurofins Genomics.

413 **Table 3.** Primer sequences for Sanger sequencing, PCR and RT-qPCR.

Primer Target	Condition	Forward (5' - 3')	Reverse (5' - 3')	Note
MYH7	Sequencing	AGACTCCCTGCTGGTAATCCAGT G	N/A	
MYH7	PCR	ATCCCTGAGGGACAGTTCATTG	GGGTTGTGGGAAGTGAAGGC	Amplifies native allele
MYH7	PCR	ATCCCTGAGGGACAGTTCATTG	GGTTGTCTTGTTCGCCTG	Amplifies knockin allele
TP53	PCR	CGCCAACCTCTCTAGCTCG	GCACCACCACACTATGTCTGA	
HPRT	RT-qPCR	TGACACTGGCAAACAATGCA	GGTCCTTTTACCAGCAAGC T	
TP53	RT-qPCR	CAGCACATGACGGAGGTTGT	TCATCCAAATACTCCACACGC	

414

415

4.8. Immunocytochemistry

416 hiPSC-CMs were seeded at 25k/cm² in Matrigel-coated 4-well chamber slides (Mil-
417 lipore, PEZGS0416) and cultured for 72h in DMEM-based cardiomyocyte culture media.
418 Cells were fixed with 4% paraformaldehyde for 5 min at room temperature and
419 permeabilized with 0.2% Triton X-100 in 1x PBS for 5 min at room temperature. Cells were
420 rinsed 2x with 1x PBS and incubated for 10 min in the dark at room temperature with
421 1:2000 Hoechst 33342 (Thermo Fisher, H3570). Cells were imaged at 40x using a custom
422 Nikon ECLIPSE Ti spinning disk confocal microscope with a Yokogawa W1 spinning disk
423 head (Yokogawa, CSU-W1), using 405 and 488 nm lasers. Images were captured using
424 Nikon NIS Elements AR software.

425

4.9. Western blot

426

4.9.1. Lysate preparation

427 Monolayer-cultured hiPSC-CMs were rinsed 2x with 1x PBS and lysed with Pierce
428 RIPA lysis buffer (Thermo Fisher, 89901) supplemented with Halt protease and phos-
429 phatase inhibitor (Invitrogen, 78443) and dithiothreitol (Roche, 3483-12-3). Lysates were
430 rocked at 4C for 20 min and centrifuged 10 min at 15,000g, with supernatant collected.
431 Total protein concentration of supernatant was assessed by Bradford assay (Bio Rad,
432 5000006) with 560 nm absorbance per manufacturer's protocol using BSA standards
433 (Thermo Fisher, 23208). Lysates were diluted with 4x Laemmli SDS Sample Buffer (Bio
434 Rad, 1610747) to 1 µg/µL total protein concentration.

435

4.9.2. Electrophoresis and staining

436 Lysates were loaded at 15 µg in Mini Protean 4-15% polyacrylamide gels (Bio Rad,
437 4508084). Electrophoresis was run at 120 V for 50 min in 1x tris-glycine-SDS running
438 buffer [25 mM tris base (Sigma, T1503-1KG), 190 mM glycine (Fisher, BP381-1), 0.1%
439 sodium dodecyl sulfate (Fisher, BP243-1)]. Proteins were transferred to Immobilon-P
440 membranes (Millipore, IPVH85R) at 120V for 65 min at 4C in 1x tris-glycine-methanol
441 transfer buffer [25 mM tris base, 190 mM glycine, 20% methanol (Fisher, A412P-4)].
442 Membranes were blocked with 5% milk (CAT) in 1x tris buffer saline with Tween-20
443 [TBST; 20 mM tris base, 150 mM Tween-20 (Sigma, P9416-100mL)] for 120 min at RT.
444 Membranes were washed 3x with 1x PBS and incubated with appropriate primary anti-
445 body (Table 4) diluted in 4% BSA (Sigma, A9418-50G) in 1x PBS overnight at 4C.
446 Membranes were washed 3x with 1x PBS and incubated with appropriate secondary anti-
447 body diluted in 1% BSA in 1x TBST for 60 min at RT. Membranes were washed 3x with

448 1x PBS and incubated with Clarity Max ECL substrate (Bio Rad, 1705061) for 5 min.
449 Chemiluminescence images were obtained using the ChemiDoc imaging system (Bio
450 Rad, 17001401). Volumetric band intensities were analyzed using Bio Rad Image Lab
451 software.

452 **Table 4.** Western blot antibodies.

Target	Species	Dilution	Vendor	Catalog Number
β MHC	Mouse	1:500	Developmental Studies Hybridoma Bank	A4.951
GFP	Goat	1:250	Novus Bio	100-1770
α -Sarcomeric Actinin	Rabbit	1:1000	Abcam	AB68167
GAPDH	Mouse	1:2000	Santa Cruz Biotechnology	SC32233
p53	Mouse	1:500	Santa Cruz Biotechnology	SC126
anti-Mouse HRP	Goat	1:2000	Bio Rad	1705047
anti-Rabbit HRP	Goat	1:2000	Bio Rad	1705046

453

4.10. TUNEL staining and analysis

454

455 hiPSC-CMs were seeded at 25k/cm² in Matrigel-coated 4-well chamber slides (Mil-
456 lipore, PEZGS0416) and cultured for 72h in DMEM-based cardiomyocyte culture media.
457 Cells were fixed with 4% paraformaldehyde and stained using the Click-IT Plus TUNEL
458 Assay kit (Invitrogen, C10619) with Alexa Fluor 647 secondary per manufacturer's pro-
459 tocol. Cells were rinsed 2x with 1x PBS and incubated for 10 min in the dark at room
460 temperature with 1:2000 Hoechst 33342. Cells were rinsed 2x with 1x PBS and imaged at
461 40x with spinning disk confocal microscopy as above with 405, 488, and 640 nm lasers.
462 Images were segmented using ImageJ and Hoechst+/TUNEL+ nuclei in EGFP+ cells
463 were quantified.

4.11. Flow cytometry and FACS

464

4.11.1. Flow cytometry

465

466 Cells were trypsinized, centrifuged, and resuspended as above. For mitochondrial
467 superoxide staining, cells were incubated with 2.5 μ M MitoSOX Red (Thermo Fisher,
468 M36008) in 100 μ L PBS for 1 h room temperature, rinsed with 1x PBS, centrifuged for 3
469 min at 300g, and resuspended in 5% FBS in PBS without fixation. For all other flow as-
470 says, cells were fixed with 4% paraformaldehyde for 5 min. For staining of patient line
471 iPSC-CMs with cardiac troponin T (cTnT), cells were incubated with cardiac troponin T
472 APC-conjugated antibody (Miltenyi Biotec, 130-120-403) or REA control human IgG1
473 APC-conjugated isotype antibody (Miltenyi Biotec, 130-120-709) for 1 h at room temper-
474 ature in the dark in 0.75% saponin (Sigma, 558255-100G) and 5% FBS in 1x PBS. Cells
475 were rinsed with 1x PBS, centrifuged for 3 min at 300g, and resuspended in 5% FBS in 1x
476 PBS for analysis using a FACSCanto cytometer. Populations were serially gated for
477 FSC-A/SSC-A, FSC-H/FSC-W, and GFP+/AmCyan- to identify EGFP-expressing
478 iPSC-CMs.

4.11.2 FACS of EHTs

479

480 At cast week 1 or week 3, EHTs were rinsed with 1x PBS and carefully removed from
481 PDMS posts using forceps. Tissues were placed in 1 mL of papain-based dissociation
482 solution [40 U/mL papain from *C. papaya* (Sigma, 76220-25G), 5.5 mM L-cysteine HCl
483 monohydrate (Sigma, C7880-500MG), 1 mM EDTA (Fisher, 02-002-790), 0.5% be-
484 ta-mercaptoethanol (Sigma, M6250), 1x PBS] (28). Tissues in dissociation solution were
485 incubated for 10 min at 37C, 5% CO₂ and gently triturated into single cells. Dissociation
486 was halted with 5% FBS in RPMI, and cells were centrifuged for 3 min at 300g and re-
487 suspended in 5% FBS in 1x PBS. 10% of cells were fixed with 4% paraformaldehyde for 5
488 min for replicate analysis by flow cytometry. The remaining cells were filtered with 40 μ m
489 filters, centrifuged for 3 min at 300g, and resuspended in 5% FBS in 1x PBS. Cells were
490 sorted using a BD FACSAria II sorter with 70 μ m nozzle, serially gating for FSC-A/SSC-A,
491 FSC-H/FSC-W, and GFP+/AmCyan- populations. Sorted cells were collected in 5% FBS
492 in 1x PBS for analysis.

493

4.12. Apoptosis antibody array

494 Monoculture differentiation day 35 hiPSC-CMs were assessed using the 43-target
495 Human Apoptosis Antibody Array (Abcam, ab134001) according to manufacturer's pro-
496 tocol. Briefly, hiPSC-CMs were lysed with provided lysis buffer and blocked membranes
497 were incubated with 200 µg lysate. Membranes were serially incubated with bio-
498 tin-conjugated anti-cytokines and streptavidin-HRP. Chemiluminescence images were
499 obtained using the ChemiDoc imaging system. Volumetric intensities were analyzed using
500 Bio Rad Image Lab software.

501 4.13. RT-qPCR

502 RNA was isolated from hiPSC-CMs with PureLink RNA minipreps (Invitrogen,
503 12183018A) with PureLink DNase treatment (Invitrogen, 12185010) per manufacturer's
504 protocol. cDNA was generated via reverse transcription using SensiFast cDNA Synthesis
505 Kit (Thomas Scientific, C755H65) per manufacturer's protocol. qPCR was performed with
506 10 µL reactions in technical triplicate and 40 cycles with SYBR Select Master Mix (Invi-
507 trogen, 4472919), 5 ng cDNA per reaction, and 100 nM of forward and reverse primer
508 (Table 3) on an ABI 7900HT Real-Time PCR machine (Fisher, 4329001).

509 4.14. Statistics

510 Statistical comparisons of cell size, forward scatter area, twitch force, cell count,
511 protein expression, and gene expression were performed using one-tail Student's T-tests
512 with unequal variances and significance criteria $p < 0.05$.

513 **Supplementary Materials:** The following supporting information can be downloaded at:
514 www.mdpi.com/xxx/s1, Figure S1: Generation of isogenic βMHC-EGFP expressing hiPSC-CMs
515 using CRISPR/Cas9 editing; Figure S2: DMEM-based cardiomyocyte media accelerates maturation
516 of hiPSC-CMs in monolayer culture; Figure S3: MYH7 E848G induces p53-associated intrinsic
517 apoptosis in monolayer and EHT culture; Figure S4: Generation of MYH7WT/E848G-EGFP TP53-/-
518 hiPSC-CMs using CRISPR/Cas9 editing; Table S1: Expression of apoptosis antibody array targets
519 associated with Figure 3A-B; Table S2: sgRNA sequences used for CRISPR/Cas9 editing of
520 hiPSCs; Table S3: Primer sequences used for PCR and RT-qPCR; Table S4: Antibodies used for
521 Western blot.

522 **Author Contributions:** A.M.L.: Conceptualization, Methodology, Validation, Formal Analysis, In-
523 vestigation, Writing – Original Draft, Writing – Review and Editing, Visualization. W-M.C.: Concep-
524 tualization, Validation, Formal Analysis, Investigation, Supervision. C.E.F.: Conceptualization, Val-
525 idation, Formal Analysis, Investigation. S-L.C.: Formal Analysis, Investigation. G.W.: Formal Anal-
526 ysis, Investigation. A.G.: Investigation. N.S.: Resources, Supervision. C.E.M.: Resources, Supervi-
527 sion, Funding Acquisition. K-C.Y.: Conceptualization, Methodology, Validation, Resources, Writing
528 – Review & Editing, Visualization, Supervision, Project Administration, Funding Acquisition. All
529 authors have read and agreed to the published version of the manuscript.

530 **Funding:** This research was funded in part by a Career Development Award (IK2 BX004642) from
531 the United States (U.S.) Department of Veterans Affairs Biomedical Laboratory R&D (BLRD) Ser-
532 vice, the John L. Locke Jr. Charitable Trust, the Jaconette L. Tietze Young Scientist Award, and the
533 Dolsen Family Fund (to K-C.Y.). Additional funding comes from the Robert B. McMillen Foundation
534 (to K-C.Y. and C.E.M.), the NIH NHLBI (1F32HL164108-01 NIH NHLBI to A.M.L.; RO1 HL149734 to
535 N.J.S.), the NIH NIAMS (P30 AR074990 to the UW Center for Translational Muscle Research), and
536 the CMAP postdoctoral fellowship (to C.E.F.).

537 **Data Availability Statement:** The data presented in this study will be openly available in FigShare
538 pending upload.

539 **Acknowledgments:** The authors acknowledge the assistance provided by the Institute for Stem
540 Cell and Regenerative Medicine (University of Washington) in generating patient-derived hiPSCs,
541 the Mike and Lynn Garvey Cell Imaging Core at the institute, directed by Dale Hailey, in confocal
542 microscopy, and the Cell Analysis Facility Flow and Imaging Cytometry Core in the Department of
543 Immunology (University of Washington) in flow cytometry.

544 **Conflicts of Interest:** The authors have no conflicts of interest to report.

545 The content is solely the responsibility of the authors and does not necessarily represent the official
546 views of the Department of Veterans Affairs or the United States Government.

547 References

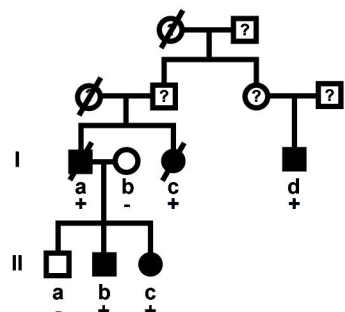
- 548 1. Ribeiro, A. J. S.; Schwab, O.; Mandegar, M. A.; Ang, Y.-S.; Conklin, B. R.; Srivastava, D.; Pruitt, B. L., Multi-Imaging Method to
549 Assay the Contractile Mechanical Output of Micropatterned Human iPSC-Derived Cardiac Myocytes. *Circ Res* **2017a**, *120*(10),
550 1572–1583. <https://doi.org/10.1161/CIRCRESAHA.116.310363>
- 551 2. Birket, M. J.; Ribeiro, M. C.; Kosmidis, G.; Ward, D.; Leitoginho, A. R.; van de Pol, V.; Dambrot, C.; Devalla, H. D.; Davis, R. P.;
552 Mastroberardino, P. G.; Atsma, D. E.; Passier, R.; Mummery, C. L., Contractile Defect Caused by Mutation in MYBPC3 Re-

- vealed under Conditions Optimized for Human PSC-Cardiomyocyte Function. *Cell Rep* **2015b**, *13*(4), 733–745. <https://doi.org/10.1016/j.celrep.2015.09.025>
- 555 3. Ma, Z.; Huebsch, N.; Koo, S.; Mandegar, M. A.; Siemons, B.; Boggess, S.; Conklin, B. R.; Grigoropoulos, C. P.; Healy, K. E.,
556 Contractile deficits in engineered cardiac microtissues as a result of MYBPC3 deficiency and mechanical overload. *Nat Biomed*
557 *Eng* **2018c**, *2*(12), 955–967. <https://doi.org/10.1038/s41551-018-0280-4>
- 558 4. Witjas-Paalberends, E. R.; Piroddi, N.; Stam, K.; van Dijk, S. J.; Oliviera, V. S.; Ferrara, C.; Scellini, B.; Hazebroek, M.; ten Cate,
559 F. J.; van Slegtenhorst, M.; dos Remedios, C.; Niessen, H. W. M.; Tesi, C.; Stienen, G. J. M.; Heymans, S.; Michels, M.;
560 Poggesi, C.; van der Velden, J.,. Mutations in MYH7 reduce the force generating capacity of sarcomeres in human familial
561 hypertrophic cardiomyopathy. *Cardiovasc Res* **2013d**, *99*(3), 432–441. <https://doi.org/10.1093/cvr/cvt119>
- 562 5. Bhagwan, J. R.; Mosqueira, D.; Chairez-Cantu, K.; Mannhardt, I.; Bodbin, S. E.; Bakar, M.; Smith, J. G. W.; Denning, C.,
563 Isogenic models of hypertrophic cardiomyopathy unveil differential phenotypes and mechanism-driven therapeutics. *J Mol Cell*
564 *Cardiol* **2020e**, *145*, 43–53. <https://doi.org/10.1016/j.yjmcc.2020.06.003>
- 565 6. Yang, K.-C.; Breitbart, A.; De Lange, W. J.; Hofsteen, P.; Futakuchi-Tsuchida, A.; Xu, J.; Schopf, C.; Razumova, M. V.; Jiao, A.;
566 Boucek, R.; Pabon, L.; Reinecke, H.; Kim, D.-H.; Ralphe, J. C.; Regnier, M.; Murry, C. E.,. Novel Adult-Onset Systolic Cardi-
567 omyopathy Due to MYH7 E848G Mutation in Patient-Derived Induced Pluripotent Stem Cells. *JACC Basic Transl Sci* **2018f**,
568 *3*(6), 728–740. <https://doi.org/10.1016/j.jacbts.2018.08.008>
- 569 7. Akhtar, M.; Elliott, P.,. The genetics of hypertrophic cardiomyopathy. *Glob Cardiol Sci Pract* b.r. *2018*(3), 36.
570 <https://doi.org/10.21542/gcsp.2018.36>
- 571 8. Marsiglia, J. D. C.; Pereira, A. C.,. Hypertrophic Cardiomyopathy: How do Mutations Lead to Disease? *Arq Bras Cardiol* **2014h**,
572 *102*(3), 295–304. <https://doi.org/10.5935/abc.20140022>
- 573 9. Spertus, J. A.; Fine, J. T.; Elliott, P.; Ho, C. Y.; Olivotto, I.; Saberi, S.; Li, W.; Dolan, C.; Reaney, M.; Sehnert, A. J.; Jacoby, D.,
574 Mavacamten for treatment of symptomatic obstructive hypertrophic cardiomyopathy (EXPLORER-HCM): health status analysis
575 of a randomised, double-blind, placebo-controlled, phase 3 trial. *Lancet* **2021i**, *397*(10293), 2467–2475.
576 [https://doi.org/10.1016/S0140-6736\(21\)00763-7](https://doi.org/10.1016/S0140-6736(21)00763-7)
- 577 10. Marstrand, P.; Han, L.; Day, S. M.; Olivotto, I.; Ashley, E. A.; Michels, M.; Pereira, A. C.; Wittekind, S. G.; Helms, A.; Saberi, S.;
578 Jacoby, D.; Ware, J. S.; Colan, S. D.; Semsarian, C.; Ingles, J.; Lakdawala, N. K.; Ho, C. Y.; null, null.,. Hypertrophic Cardi-
579 omyopathy With Left Ventricular Systolic Dysfunction. *Circulation* **2020j**, *141*(17), 1371–1383.
580 <https://doi.org/10.1161/CIRCULATIONAHA.119.044366>
- 581 11. Hang, T.; Huang, Z.; Jiang, S.; Gong, J.; Wang, C.; Xie, D.; Ren, H.,. Apoptosis in Pressure Overload-Induced Cardiac Hyper-
582 trophy Is Mediated, in Part, by Adenine Nucleotide Translocator-1. *Ann Clin Lab Sci* **2006k**, *36*(1), 88–95.
- 583 12. Ino, T.; Nishimoto, K.; Okubo, M.; Akimoto, K.; Yabuta, K.; Kawai, S.; Okada, R.; Sueyoshi, N.,. Apoptosis as a Possible Cause
584 of Wall Thinning in End-Stage Hypertrophic Cardiomyopathy. *American Journal of Cardiology* **1997l**, *79*(8), 1137–1141.
585 [https://doi.org/10.1016/S0002-9149\(97\)00066-0](https://doi.org/10.1016/S0002-9149(97)00066-0)
- 586 13. Kang, P. M.; Izumo, S.,. Apoptosis and Heart Failure. *Circulation Research* **2000m**, *86*(11), 1107–1113.
587 <https://doi.org/10.1161/01.RES.86.11.1107>
- 588 14. Sabbah, H. N.,. Apoptotic cell death in heart failure. *Cardiovascular Research* **2000n**, *45*(3), 704–712.
589 [https://doi.org/10.1016/S0008-6363\(99\)00348-X](https://doi.org/10.1016/S0008-6363(99)00348-X)
- 590 15. van Empel, V. P. M.; De Windt, L. J.,. Myocyte hypertrophy and apoptosis: a balancing act. *Cardiovascular Research* **2004o**,
591 *63*(3), 487–499. <https://doi.org/10.1016/j.cardiores.2004.02.013>
- 592 16. Wang, Y.; Huang, S.; Sah, V. P.; Ross, J.; Brown, J. H.; Han, J.; Chien, K. R.,. Cardiac Muscle Cell Hypertrophy and Apoptosis
593 Induced by Distinct Members of the p38 Mitogen-activated Protein Kinase Family. *Journal of Biological Chemistry* **1998p**,
594 *273*(4), 2161–2168. <https://doi.org/10.1074/jbc.273.4.2161>
- 595 17. Cohn, R.; Thakar, K.; Lowe, A.; Ladha, F. A.; Pettinato, A. M.; Romano, R.; Meredith, E.; Chen, Y.-S.; Atamanuk, K.; Huey, B. D.;
596 Hinson, J. T.,. A Contraction Stress Model of Hypertrophic Cardiomyopathy due to Sarcomere Mutations. *Stem Cell Reports*
597 **2019q**, *12*(1), 71–83. <https://doi.org/10.1016/j.stemcr.2018.11.015>
- 598 18. Li, J.; Zeng, J.; Wu, L.; Tao, L.; Liao, Z.; Chu, M.; Li, L.,. Loss of P53 regresses cardiac remodeling induced by pressure overload
599 partially through inhibiting HIF1 α signaling in mice. *Biochemical and Biophysical Research Communications* **2018r**, *501*(2),
600 394–399. <https://doi.org/10.1016/j.bbrc.2018.04.225>
- 601 19. Mak, T. W.; Hauck, L.; Grothe, D.; Billia, F.,. p53 regulates the cardiac transcriptome. *Proceedings of the National Academy of*
602 *Sciences* **2017s**, *114*(9), 2331–2336. <https://doi.org/10.1073/pnas.1621436114>
- 603 20. Huang, C.-Y.; Pai, P.-Y.; Kuo, C.-H.; Ho, T.-J.; Lin, J.-Y.; Lin, D.-Y.; Tsai, F.-J.; Padma, V. V.; Kuo, W.-W.; Huang, C.-Y.,
604 p53-mediated miR-18 repression activates HSF2 for IGF-1IR-dependent myocyte hypertrophy in hypertension-induced heart
605 failure. *Cell Death Dis* **2017t**, *8*(8), e2990–e2990. <https://doi.org/10.1038/cddis.2017.320>
- 606 21. Qi, X.; Han, J.; Zhao, P.; Dong, X.; Gong, S.,. S100A4 and P53 in myocardial collagen fibers of hypertrophic cardiomyopathy: L:
607 Expression and clinical significance. *Herz* **2016u**, *41*(6), 530–533. <https://doi.org/10.1007/s00059-015-4397-x>
- 608 22. Birks, E. J.; Latif, N.; Enesa, K.; Folkvang, T.; Luong, L. A.; Sarathchandra, P.; Khan, M.; Ova, H.; Terracciano, C. M.; Barton,
609 P. J. R.; Yacoub, M. H.; Evans, P. C.,. Elevated p53 expression is associated with dysregulation of the ubiquitin-proteasome
610 system in dilated cardiomyopathy. *Cardiovascular Research* **2008v**, *79*(3), 472–480. <https://doi.org/10.1093/cvr/cvn083>
- 611 23. Veeroju, S.; Mamazhakypov, A.; Rai, N.; Kojonazarov, B.; Nadeau, V.; Breuils-Bonnet, S.; Li, L.; Weissmann, N.; Rohrbach, S.;
612 Provencher, S.; Bonnet, S.; Seeger, W.; Schermuly, R.; Novoyatleva, T.,. Effect of p53 activation on experimental right ven-
613 tricular hypertrophy. *PLoS One* **2020w**, *15*(6), e0234872. <https://doi.org/10.1371/journal.pone.0234872>
- 614 24. Aubrey, B. J.; Kelly, G. L.; Janic, A.; Herold, M. J.; Strasser, A.,. How does p53 induce apoptosis and how does this relate to
615 p53-mediated tumour suppression? *Cell Death Differ* **2018x**, *25*(1), 104–113. <https://doi.org/10.1038/cdd.2017.169>
- 616 25. Ommen, S. R.; Mital, S.; Burke, M. A.; Day, S. M.; Deswal, A.; Elliott, P.; Evancovich, L. L.; Hung, J.; Joglar, J. A.; Kantor, P.;
617 Kimmelstiel, C.; Kittleson, M.; Link, M. S.; Maron, M. S.; Martinez, M. W.; Miyake, C. Y.; Schaff, H. V.; Semsarian, C.; Sorajja,
618 P.,. 2020 AHA/ACC Guideline for the Diagnosis and Treatment of Patients With Hypertrophic Cardiomyopathy: A Report of the
619 American College of Cardiology/American Heart Association Joint Committee on Clinical Practice Guidelines. *Circulation*
620 **2020y**, *142*(25), e558–e631. <https://doi.org/10.1161/CIR.0000000000000937>

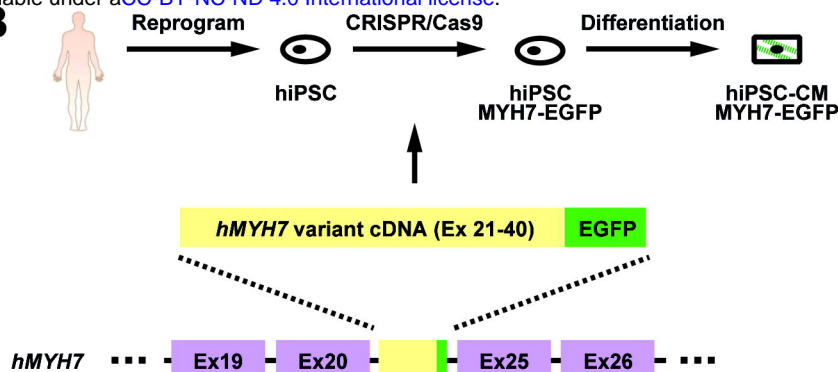
- 621 26. Leonard, A.; Bertero, A.; Powers, J. D.; Beussman, K. M.; Bhandari, S.; Regnier, M.; Murry, C. E.; Sniadecki, N. J.,. Afterload
622 promotes maturation of human induced pluripotent stem cell derived cardiomyocytes in engineered heart tissues. *J Mol Cell*
623 *Cardiol* **2018z**, *118*, 147–158. <https://doi.org/10.1016/j.yjmcc.2018.03.016>
- 624 27. Ronaldson-Bouchard, K.; Ma, S. P.; Yeager, K.; Chen, T.; Song, L.; Sirabella, D.; Morikawa, K.; Teles, D.; Yazawa, M.;
625 Vunjak-Novakovic, G.,. Advanced maturation of human cardiac tissue grown from pluripotent stem cells. *Nature* **2018aa**,
626 *556*(7700), 239–243. <https://doi.org/10.1038/s41586-018-0016-3>
627

628 **Disclaimer/Publisher's Note:** The statements, opinions and data contained in all publications are solely those of the individual
629 author(s) and contributor(s) and not of MDPI and/or the editor(s). MDPI and/or the editor(s) disclaim responsibility for any injury to
630 people or property resulting from any ideas, methods, instructions or products referred to in the content.

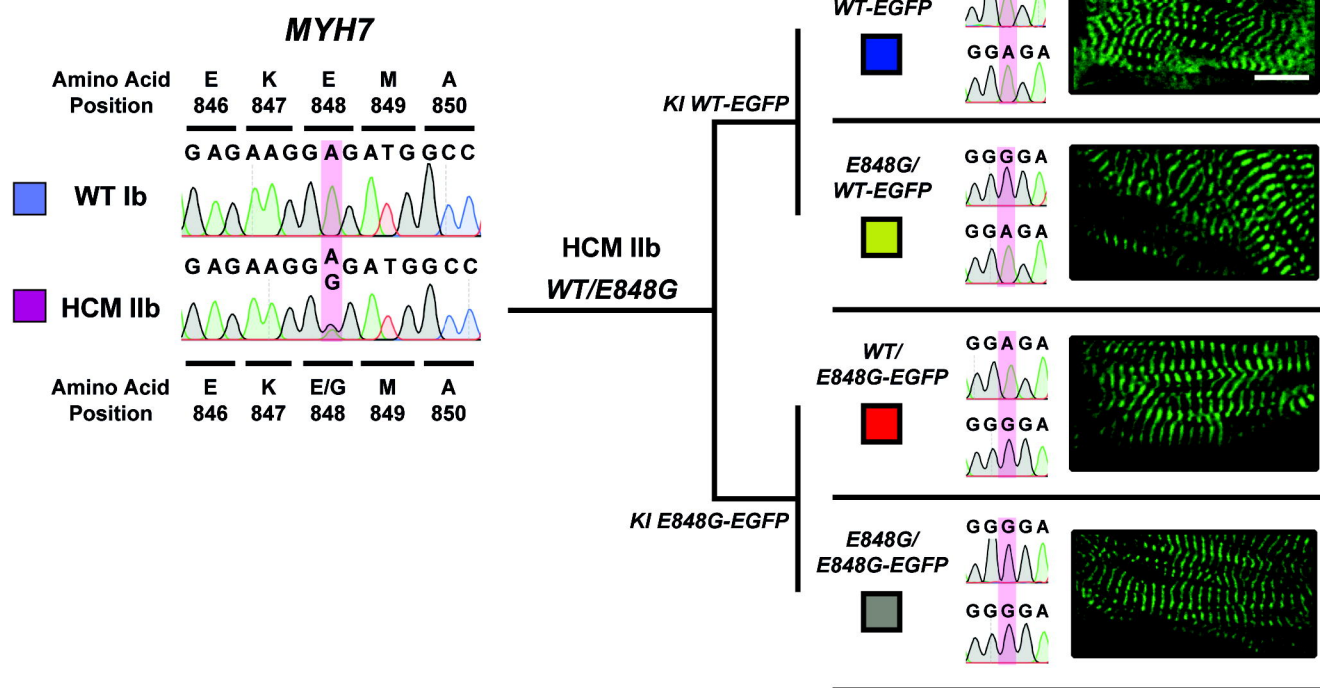
A



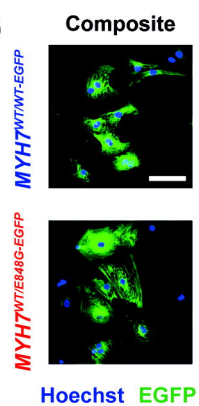
B



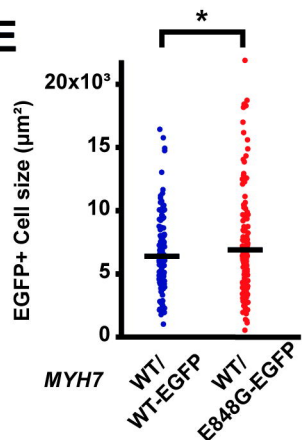
C



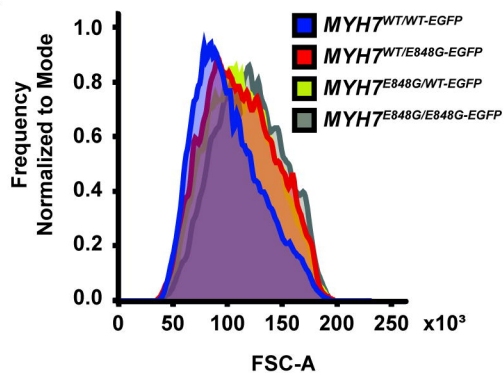
D



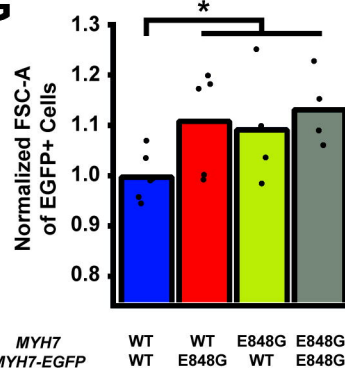
E



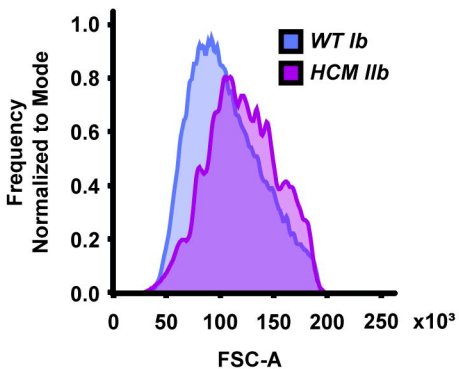
F



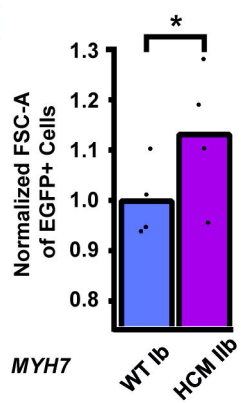
G



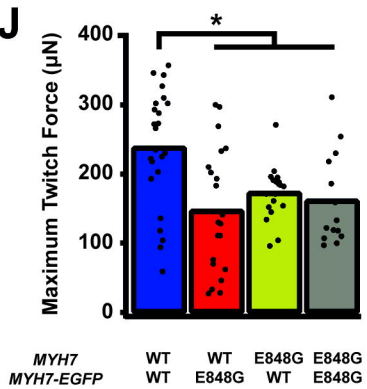
H



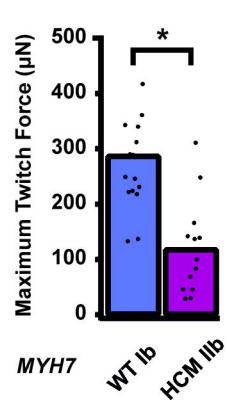
I

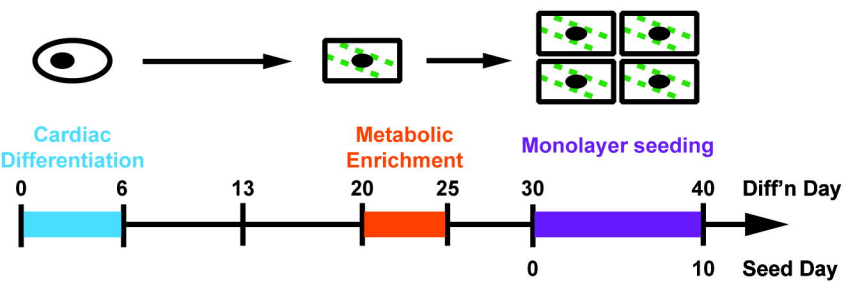
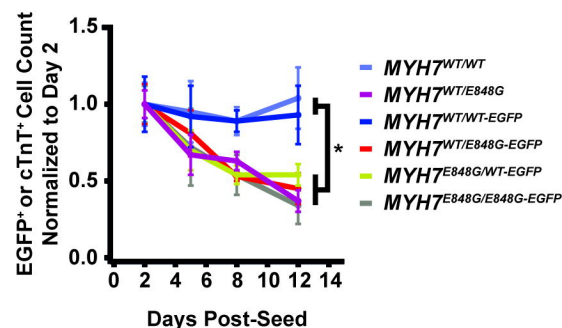
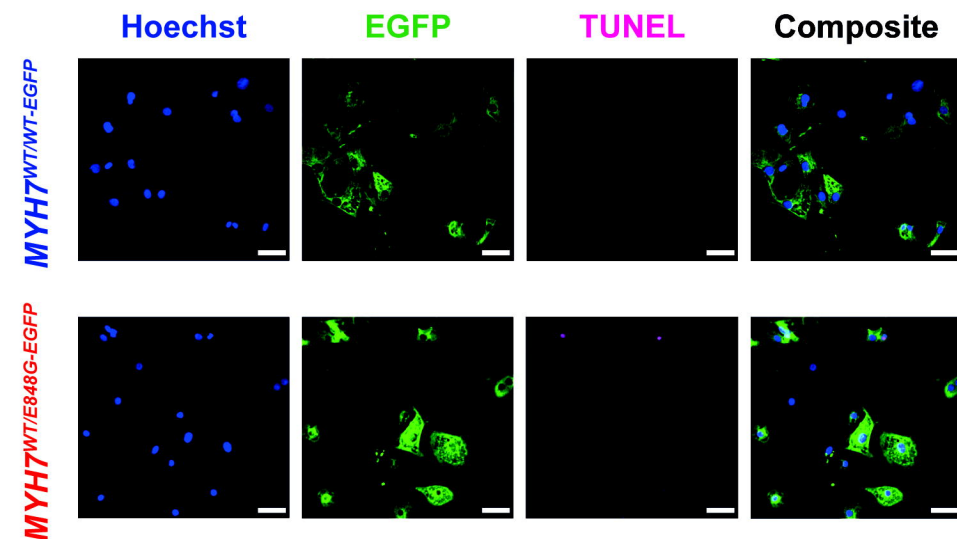
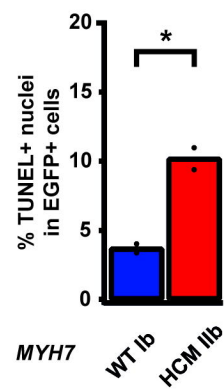
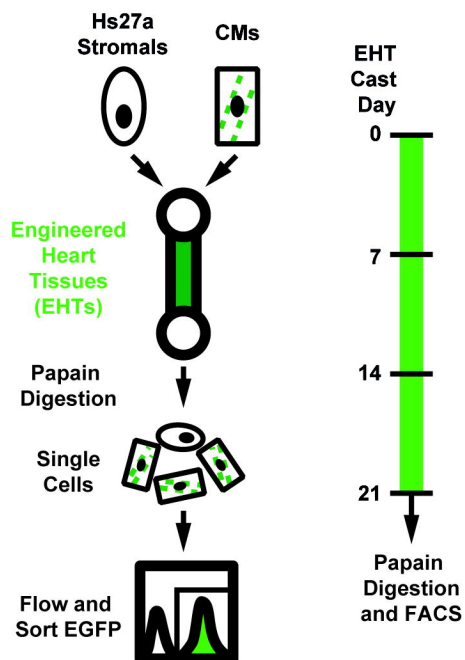
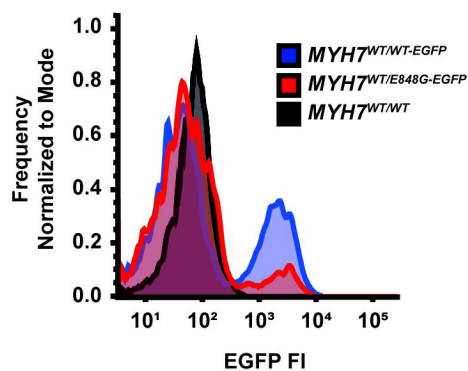
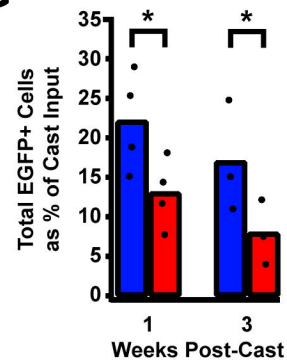
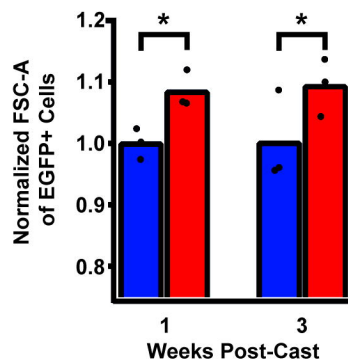


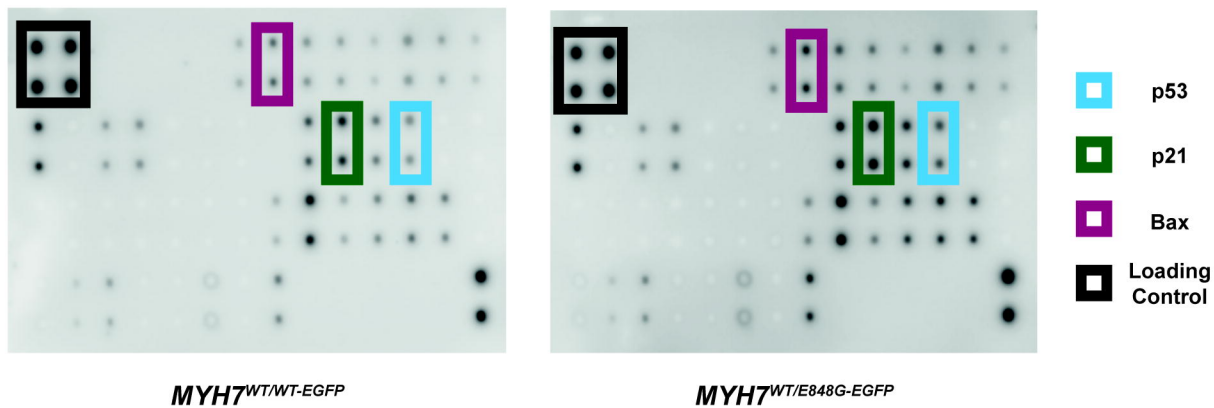
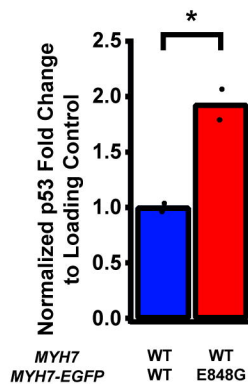
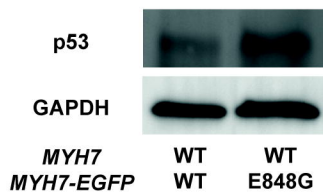
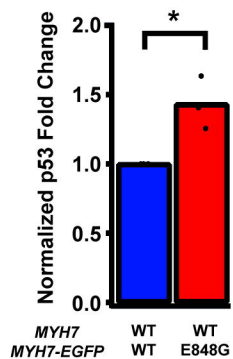
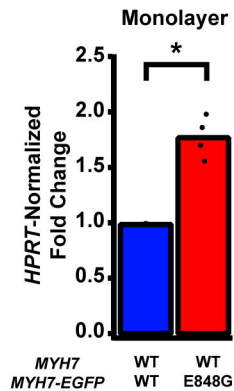
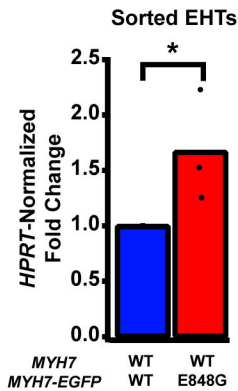
J

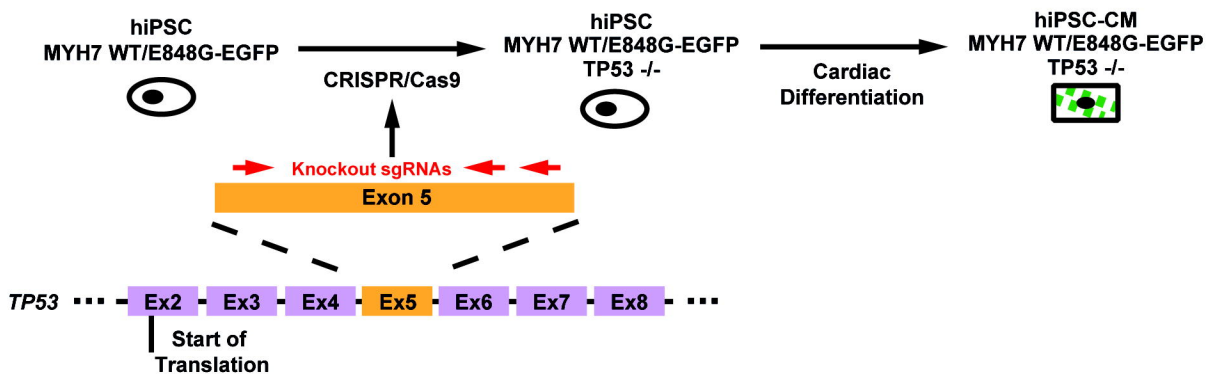
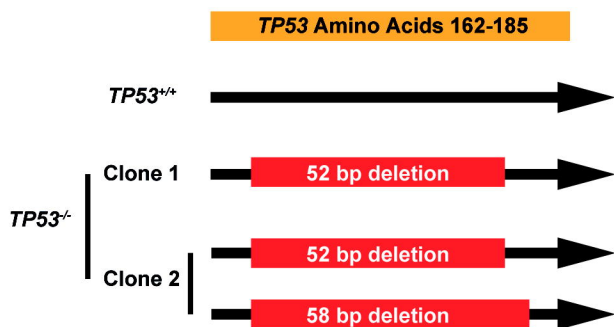
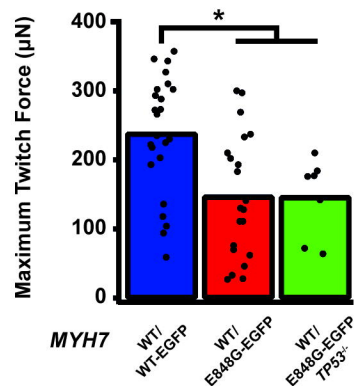
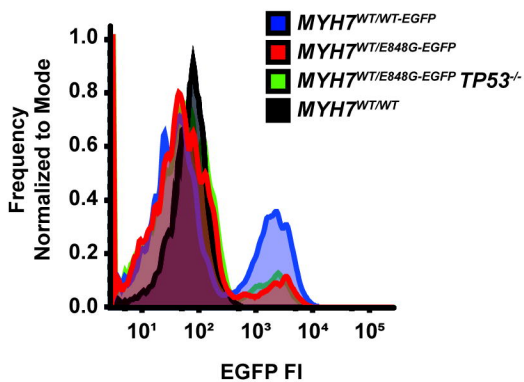
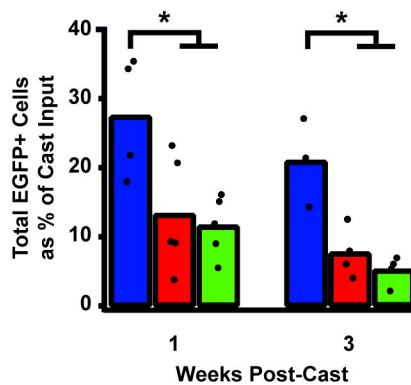


K



A**B****C****D****E****F****G****H**

A**B****C****D****E****F**

A**B****C****D****E****F**